MARY KAY O'CONNOR PROCESS SAFETY CENTER
TEXAS A&M ENGINEERING EXPERIMENT STATION

18th Annual International Symposium
October 27-29, 2015 • College Station, Texas

Effect of Moisture Content on Dust-Layer Dispersion Behind a Moving Shock Wave

H. Greg Johnston[a], Amira Y. Chowdhury[b]
M. Sam Mannan[b], and Eric L. Petersen[a]

a Department of Mechanical Engineering, Texas A&M University, College Station, TX 77843 USA

b Mary Kay O'Connor Process Safety Center, Texas A&M University, College Station, TX 77843, USA

Contact details:
E-mail:*epetersen@tamu.edu*
3123 TAMU
Phone: 979-845-1257 Fax: 979-845-3081

Abstract

Secondary dust explosions in coal mines or industrial settings are known to cause greater catastrophic hazards than the coupled primary explosions themselves. The shock waves produced during a primary explosion, which are initiated by inadvertent stimuli in an explosive atmosphere such as methane, lift surrounding coal particles from neighboring areas, and if added in an effort to create an inert mixture, limestone as well. This experimental study works with limestone dust, as its density is close to that of coal particles and its likely presence in the hazardous environment. The current study explored limestone moisture content to understand its effect on dust dispersion, which ultimately can influence the severity of a secondary explosion. A shock tube modified to evaluate dust dispersion provides the optical access to characterize the shock-wave / dust-layer interaction. Based on three shock Mach numbers, namely M_s = 1.1, 1.23, and 1.4, the trending data show an average increase of 10% in overall lifting heights and 20% in initial linear growth rates for the moisture-reduced, dried samples, as compared to undried samples stored in standard temperature and pressure (STP) conditions. Conceivably, the effective moisture reduction in the samples led to fewer agglomerations and/or reduced densities, influencing the ability of lift forces to act on the particles. The quantification of weight loss and weight differences between dried and undried samples was compared. The dust-layer rise height was measured with respect to time after the shock passage, where regardless of moisture content

in the samples, initial dust growth rates increased with Mach number. Laminar and unstable regimes were also identified in the data samples, as seen in previous studies by the authors.

1. Introduction

Environments which contain combustible dust, such as coal mines, are exposed to secondary explosion hazards, which are initiated and coupled to primary explosions in explosive atmospheres such as methane. Mitigating strategies for secondary explosion hazards are understood from the experimental data produced herein when coupled with selected gases which are the energy sources for the primary explosion, and hence produce the shock-waves that lift the dust into the atmosphere. Shock-waves lift the coal into the air, produce heat, and lead to secondary explosions or even detonations after igniting the dispersed coal particles. Specifically, experiments presented herein varied the moisture content in the dust to quantify its effect on dust dispersion with varied shock-wave speeds. Limestone dust samples were targeted for evaluation for its likely presence in the environment, inert properties, and its density being near coal dust.

In his review paper, Eckhoff [1] discussed prevention and mitigation efforts for secondary explosion hazards along with the importance of modeling dust dispersion in predicted environments. Knowledge of critical dust coverage which would lead to catastrophic explosions is needed to set safety standards. Current methods to mitigate explosive atmospheres include spreading limestone in these areas to create an inert mixture if such an accident were to occur, therefore limiting the possibility of a secondary explosion. Being able to predict or model numerically the dust dispersion behind a passing normal shock wave is therefore important, and high-quality experimental data are needed to validate such models. Dust-layer surface depth, particle density, and moisture content do have important effects on the lifting height, as their affects are illustrated herein.

To predict dust-layer entrainment into the post-shock gas flow, it is important to understand the initial motion of the particles. Previous work has been performed to enrich the fundamental knowledge of dust dispersion. However, it is still difficult to completely describe the dust entrainment mechanism. A conclusive model to accurately simulate the exact entrainment process has yet to be developed, although some recent numerical models that capture the details of the shock-dust interaction are appearing in the literature [2,3]. Therefore, to ensure safety regarding dust explosion hazards, it is important to study the dust-lifting process experimentally and identify important parameters that will be valuable for development and validation of numerical predictions of this phenomenon. Former experimental works have studied the interaction of unsteady dust layers with different elements of gas-dynamic flows (e.g., shock, compression, and expansion waves).

Earlier shock and dust particle interaction experiments focused on understanding the phenomenon of dust lifting [3]-[11]. For example, Fletcher's [5] explanation of the mechanism of dust lifting was based on experiments as well as theoretical analysis. He criticized Gerrard's [4] conclusion that dust entrainment is under the action of a shock wave passing through the dust layer. Instead, he concluded that the dust is lifted by the rapid flow behind the propagating shock. Bracht and Merzkirch [6] identified the governing force in dust lifting as the Saffman force and supported their experimental work with a numerical model. The behavior of a coal-dust layer with a weak shock wave passing above it was studied by Hwang [7]; the coal dust particle size was up to 44 μm in this work. Later, the effect of particle size on dust dispersion [8] and Magnus force [9] were studied. Fedorov [10] in his review paper discussed the significant body of work related to shock interaction with dust layers. According to Federov's conclusion, the dust lifting from a packed bed does not depend on the layer depth. However, curving of the layer surface and particle density does have important effects on the lifting height.

Some of the other studies focused on the dust-lifting problem in conjunction with combustion problems and with detonation, which is usually called a layered detonation. In 2005 and 2012, Klemens et al. studied shock interaction with coal dust and silica dust in a shock tube to identify important parameters such as the time delay in lifting the dust from the layer and the dust concentration gradient behind the propagating shock [11]. For the numerical part of their research, they considered two approaches: Eulerian and Lagrangian for modeling the dispersion of coal dust.

In spite of all the efforts, it is still difficult to describe the dust entrainment mechanism, and moreover, detailed data are still needed. As a result, a comprehensive model to simulate the exact entrainment process is yet to be demonstrated. The processes of dust lifting and two-phase flows were also comprehensively studied numerically [1,2,10-19]. Nonetheless, there is no mathematical model that can describe all stages of the process of dust lifting, including the propagation of waves on the layer, the processes of turbulent mixing, and the specific features of the force interaction of the phases [10]. However, using an Eulerian framework for computation, the very recent Houim and Oran [2] results trended well with early data from the facility described herein at M = 1.4 that were presented at a conference in 2014. Such a result shows promise in the ability to eventually model the phenomenon and the need for data such that the facility described in the present paper can provide. In addition, advancements in high-speed imaging have made possible the accumulation of large amounts of time-dependent dust-layer growth data.

With these issues is mind, the study of shock waves over dried and undried dust layers has been developed by the authors. The shock tube has optical access to provide high-speed flow visualization using a simple shadowgraph technique. Also, a direct photographic technique was synchronized with the shock wave motion to track the motion of the dust-air interface. This paper is divided as follows. First, the details of the experimental setup are described, including the shock-tube facility, dust-layer setup and material characterization, and measurement techniques for data reduction. Finally, discussion of the results is presented.

2. Experimental Setup

This section consists of the details of the shock-tube hardware and the procedures for performing the shock-wave/dust-layer interaction experiments. Described first is the shock-tube facility. Next, details on the technique for quantitative measurement of the dust-layer height as a function of time are discussed using high-speed imaging and custom photo processing. Finally, the dust-layer setup and undried limestone material characterization are discussed. Detailed assessment of the shock tube is discussed in Chowdhury et al. [20].

2.1 Shock-Tube Facility

The shock tube is ideal because its driven section is square in cross section. The key features of the test section are a large-windowed region for viewing the experiment. The test section is designed to handle incident-shock velocities up to $M_s = 2$ with an initial pressure of 1 atm (101.3 kPa), and it is capable of holding pressures up to 15 atm (1.52 MPa) behind the reflected shock wave. A schematic of the shock tube is provided in Fig. 1.

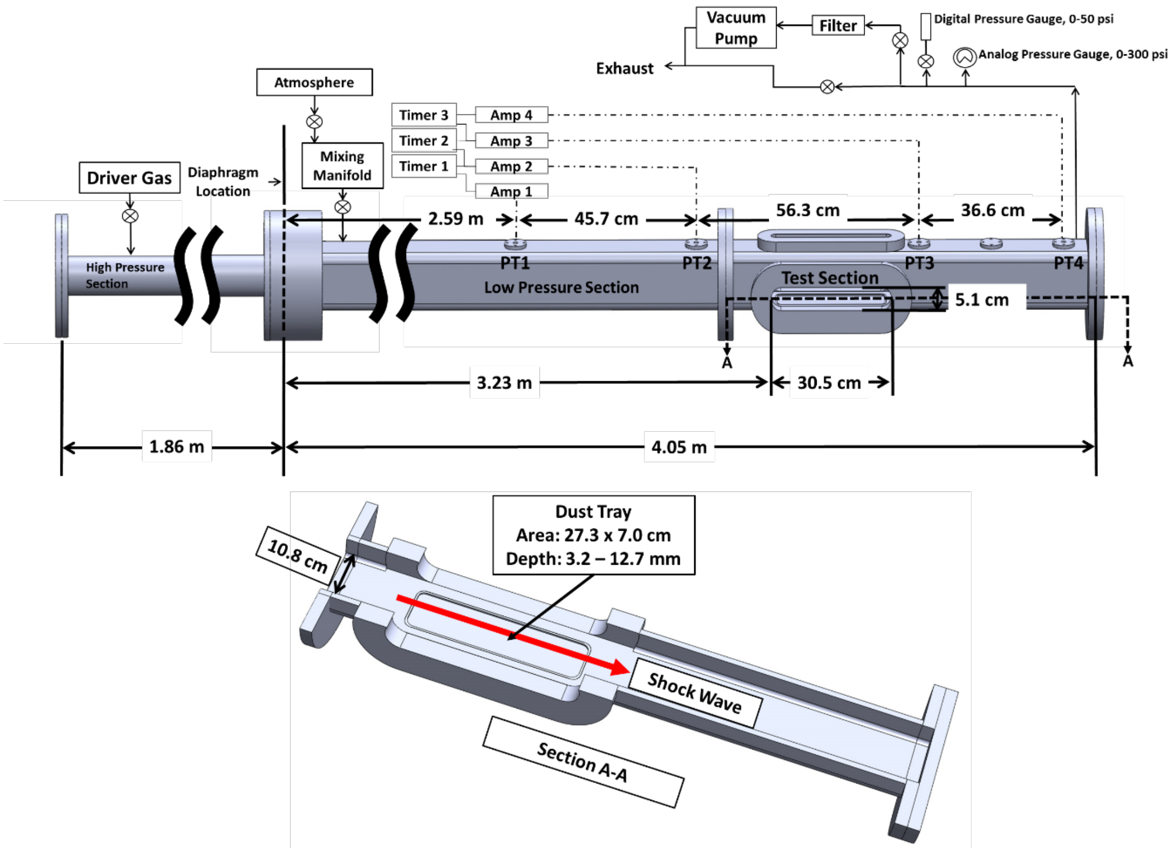

Fig. 1 Shock-tube schematic (top) showing plumbing, relative distances, test-port location, 4 pressure transducers (PT1 – PT4), 3 velocity-detection timers, and section-cut of the dust-layer test section (bottom).

Figure 1 (in the section view) shows the test section located at the end of the shock tube where the dust is leveled coincident with the incident shock wave path. Care is taken to create a uniform layer while minimizing compaction. At nominal test Mach numbers, experiments up to 3 ms are achieved. The driven section, where the dust-layer test section is located, is approximately 10.8×10.8 cm and 4.05 meters long. The left and right windows are each 5.1×30.5 cm and allow for viewing of the dust layer and fluid interface, particularly for shadowgraph techniques. Dust is placed in an easy-to-remove dust pan with a dust deposit area of 27.3×7.0 cm. Figure 2 shows a photograph of the shock-tube facility test section.

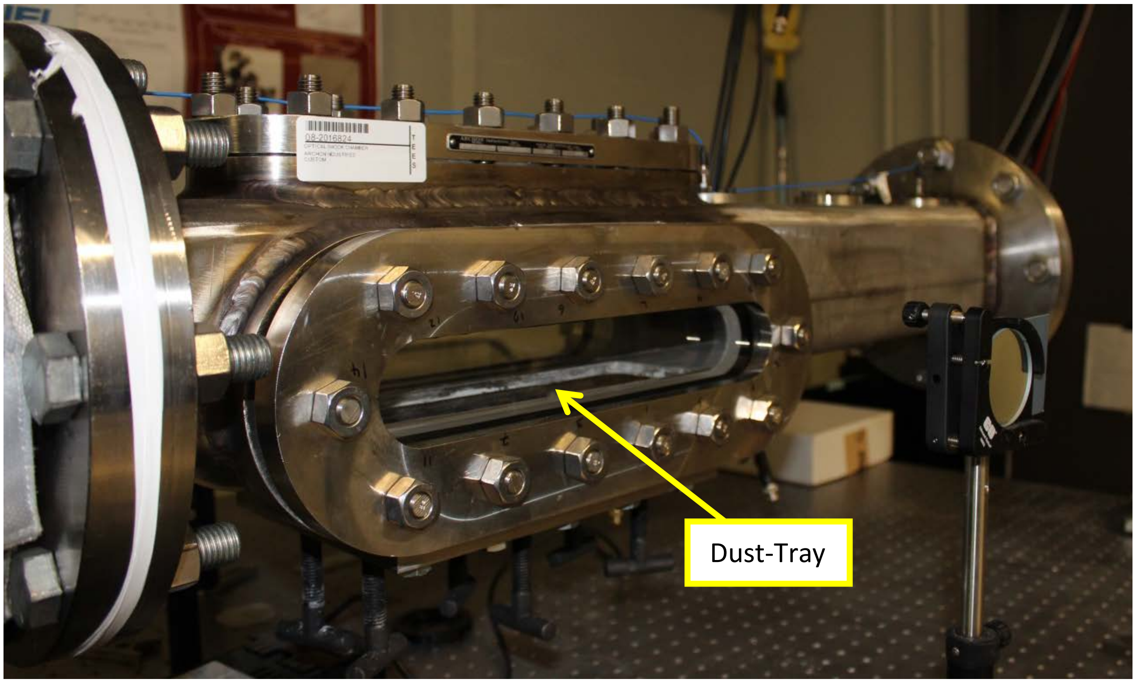

Fig. 2 Photograph of shock-tube test section.

The shock velocity is determined by a series of pressure transducers connected to three timing gates (Fluke PM6666 counters), depicted schematically in Fig. 1. Of the three timing intervals, one is before the dust-layer test section, one spans the test section, and one is after the test section.

2.2 Dust-Layer Measurement Technique

A basic shadowgraph technique was employed for flow field visualization. The present experimental viewing area is approximately 76 mm wide by 50 mm high, with the image width being limited by the concave mirror diameter and the image height by the height of the window. The curved mirrors have a 76-mm diameter and 44-cm focal length, resulting in a F# of 5.8. A Photron Fastcam SA1.1 high-speed camera at a frame rate of 15,000 fps and 1-μs exposure is used in conjunction with a Mercury-Xenon, 70-W lamp to capture the fluid and dust layer interaction. This framing rate provides a 67-μs time difference between each image. The camera was set to an image area resolution of 768×624 pixels, with a measurement tolerance of $\pm$0.09mm.

To understand dust-layer entrainment into the post-shock gas flow, particle lifting is typically measured with respect to time or with respect to the shock-wave propagation. For each experiment, images are captured of the air and dust-layer interaction behind the incident shock wave. A typical image sequence of the dust-air interaction behind a shock wave of M_s = of 1.32 is shown in Fig. 3. It can be observed that a normal shock wave is followed by the subsequent movement of the dust layer in the vertical, or y, direction. Note that the shadowgraph method provides a very good resolution of the boundary between the edge of the bulk dust layer and the gas above it, particularly for the earlier portion of the experiment. Dust surface-layer transition to instability occurs from image (c) to (d), as this is indicative of all experimental runs occurring at different times depending on the shock speed. As seen in the last frame of Fig. 3, the reflected shock wave arrives at the test section, and the data acquisition portion of the experiment is concluded.

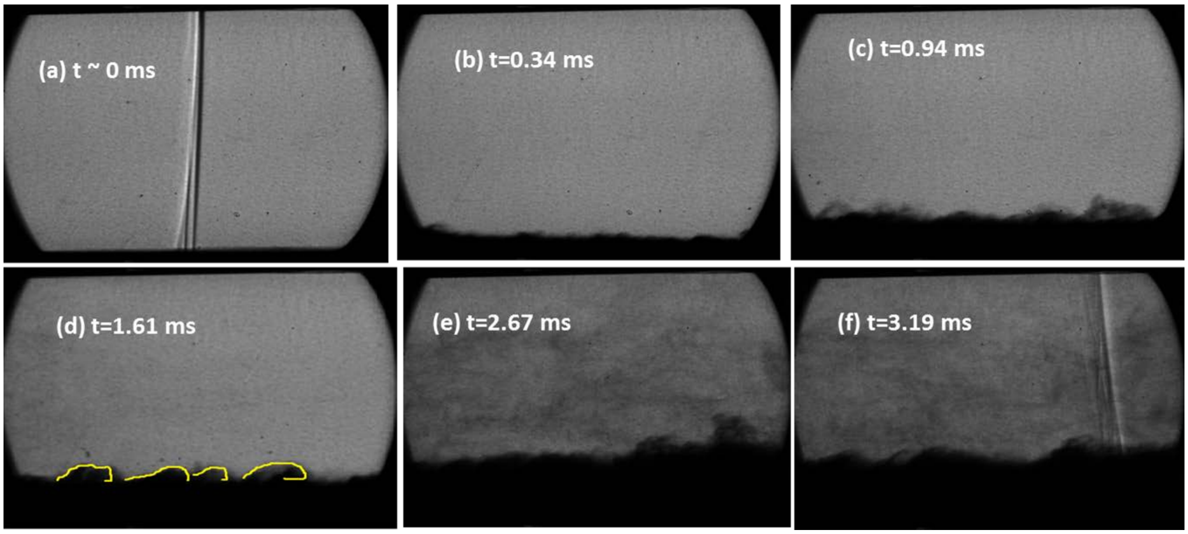

Fig. 3 Images of air and limestone dust interaction in the flow behind a shock; M_s = 1.32. All captured images were for 15,000 frames per second with a 1-µs exposure time.

Dust height as a function of time is determined by examining the shadowgraph images. The corresponding shock wave propagation was derived from the shock velocity and time recorded by the camera using a known camera trigger location, which in the present tests is the pressure transducer upstream of the window, PT1 (see Fig. 1).

The initial and subsequent images taken during the experiments were analyzed frame-by-frame for spatially and temporally dependent dust measurements. Image analysis was performed by an in-house MATlab code designed to examine pixel-to-pixel variation and to identify the location of dust-air boundaries and shock waves. To discern and measure a clear dust-air boundary for recording dust-height variation, the images were converted from raw, indexed values to RGB. Pixel RGB values were examined to set thresholds correlating to shadowgraph density gradients.

2.3 Dust-Layer Setup and Material Characterization

Experimental variables from test to test include initial pressure (P_1), shock Mach number (M_s), dust-layer thickness, and dried and undried characteristics of the dust itself. A constant value of 67 kPa (500 torr) was used for P_1 herein, or initial test section pressure. For the test gas, air was used. After each experiment that employed dust, the inner surfaces of the shock tube were cleaned thoroughly with acetone. The dust-layer depth remained constant at 3.2 mm with the geometry shown in Fig. 1 throughout the experiments.

For the present study, dust layers are limestone dust obtained off-the-shelf. The SEM images and a Beckman coulter counter assessment suggested an average particle size of 4.2 microns. Figure 4 displays SEM images of the undried limestone dust particles used in some of the experiments described herein.

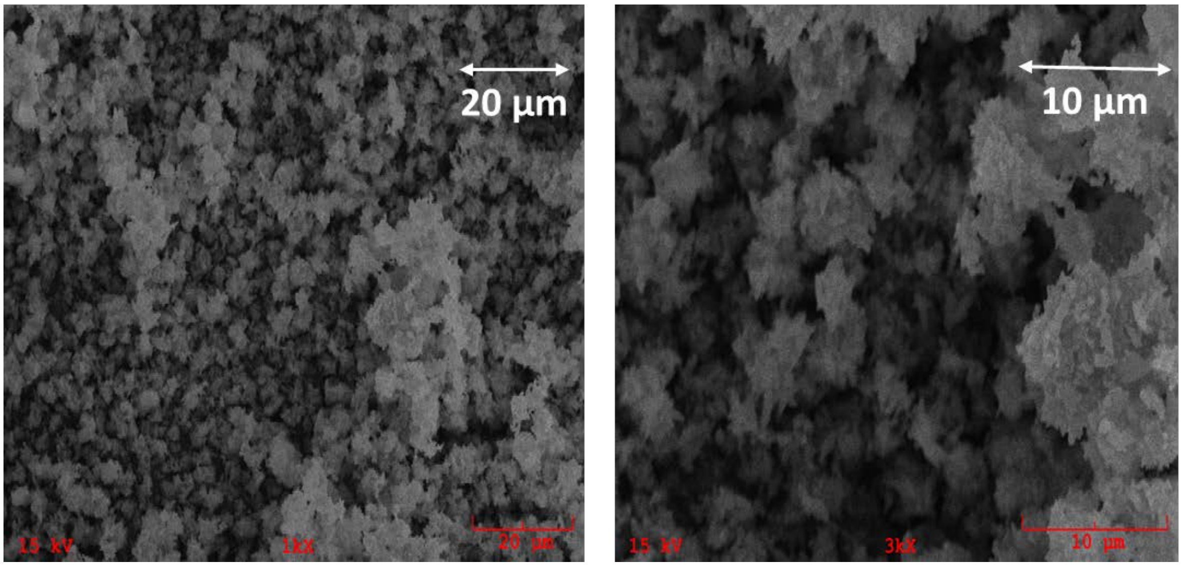

Fig. 4 SEM images of the undried limestone powder utilized herein, at two different magnifications. Average particle sizes closer to the measured value of 4.2 microns are evident in the image, with some agglomerations of approximately 20-30 microns, which may affect dust lifting height in contrast to a homogenous 4.2 micron or dried mixture.

3. Results and Conclusion

This section consists of the results and conclusions presented for both the dried and undried limestone samples at varying Mach numbers. Described first are the results of the dust dispersion tests conducted with M_s = 1.1, 1.23, and 1.4, with emphasis on moisture content differences. Next, conclusions are drawn from the presented results.

The weight data for the dried samples were recorded in Table 1, and moisture content for the dried samples were calculated in accordance with Equation 1.

$$Percent\ Moisture\ Content = \frac{Wet\ Weight - Dry\ Weight}{Wet\ Weight} \times 100 \qquad \text{(Equation 1)}$$

Table 1 Average weight and moisture content in several dried limestone samples for respective Mach number testing.

Mach Number	Sample Weight (grams)	Moisture Content
1.1	17.01	0.52%
1.23	19.845	1.02%
1.4	24.81	1.00%

Average sample weights and percent moisture content are shown in Table 1 for multiple dried limestone samples which were tested for dust dispersion at the respective Mach numbers shown. Positive numbers indicate the moisture content removed from the samples prior to the experiments. All samples were dried at elevated temperatures for approximately 192 hours.

3.1 Results

The results represent the differing of dust dispersion heights due to the dried and undried limestone samples and shock Mach number. Figure 5 illustrates the dust height growth over time for different Mach numbers. Based on the three Mach numbers, namely 1.1, 1.23, and 1.4, the trending data show an increase in lifting height for the dried samples, as compared to the undried samples. Dried sample dust heights varied from -30 to +32, -15 to +44, and -36 to +45 percent differences from undried samples for M_s = 1.1, 1.23, and 1.4, respectively. The majority of the data points are greater values for the dried samples. The solid lines in Fig. 5 represent initial linear growth rates, or $\frac{d(Y_d)}{dt}$, where the dust-air boundary layers remain laminar. The growth rates are larger for the dried samples, as compared to the undried samples.

When the dust-layer height is plotted as a function of time, the initial trend appears to be linear, as seen in Fig. 5. However, at some later time (about 2 ms for M_s = 1.23) the rate of growth slows down considerably. In this second regime, note also that the data representing the dust-layer height have much larger scatter, due primarily to the surface structures that begin to appear.

Figure 5 also illustrates the transition from the higher growth rate to the lower one appearing to be dependent on the shock Mach number, where the higher M_s leads to a transition point at earlier times when compared to the lower M_s cases. These results are typical of the experiments performed to date in the facility [20]. The transition points appear to be reduced for the dried samples at M_s = 1.1 and 1.23, with M_s = 1.4 following the opposite trend.

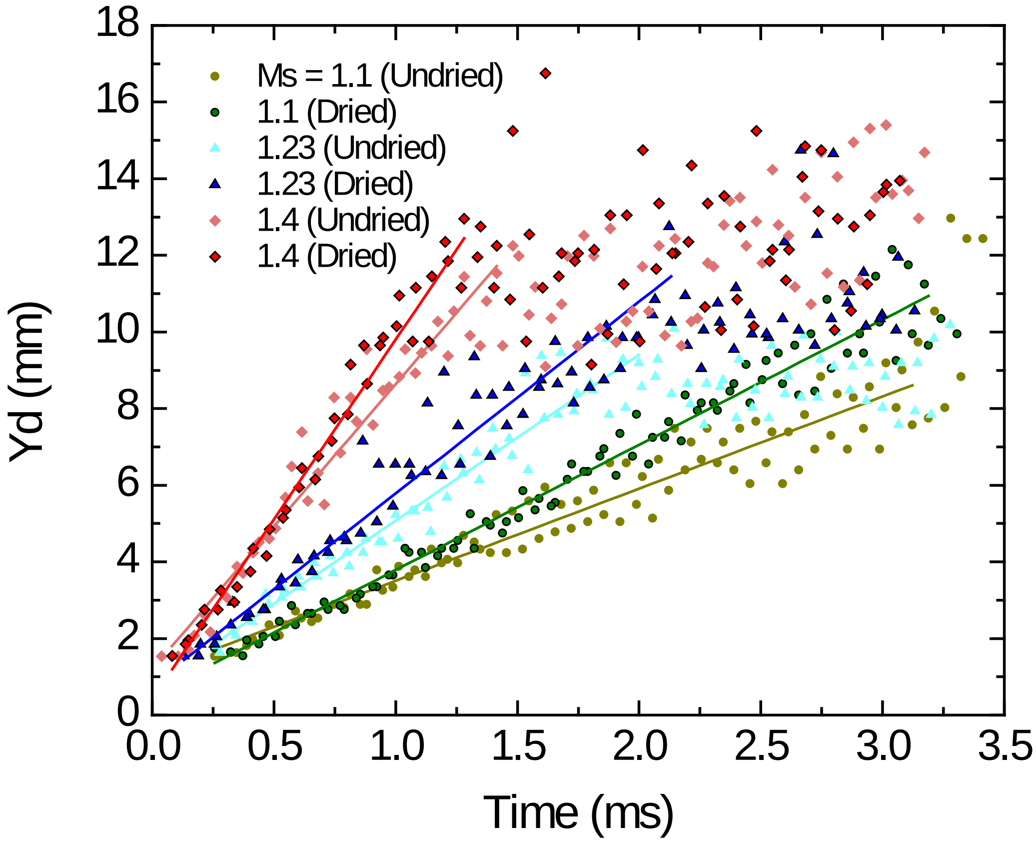

Fig. 5 Dried and undried limestone sample comparison for measured dust-layer height, Y_d, as a function of time for three different M_s (1.1, 1.23, and 1.4). Dried sample linear growth regimes (solid lines) increase in the laminar regions, as compared to the undried samples at the corresponding Mach numbers.

In Fig. 6, correlations were developed from the linear growth height regions for a given shock Mach number, M_s. Linear growth rates varied from 3.27 to 2.4, 5 to 4.3, and 9.4 to 7.4 mm/ms for M_s = 1.1, 1.23, and 1.4, respectively; where the larger values at specific Mach numbers were the dried samples. Clearly, the dried samples are rising faster and maintaining larger overall dust height values at the corresponding Mach numbers.

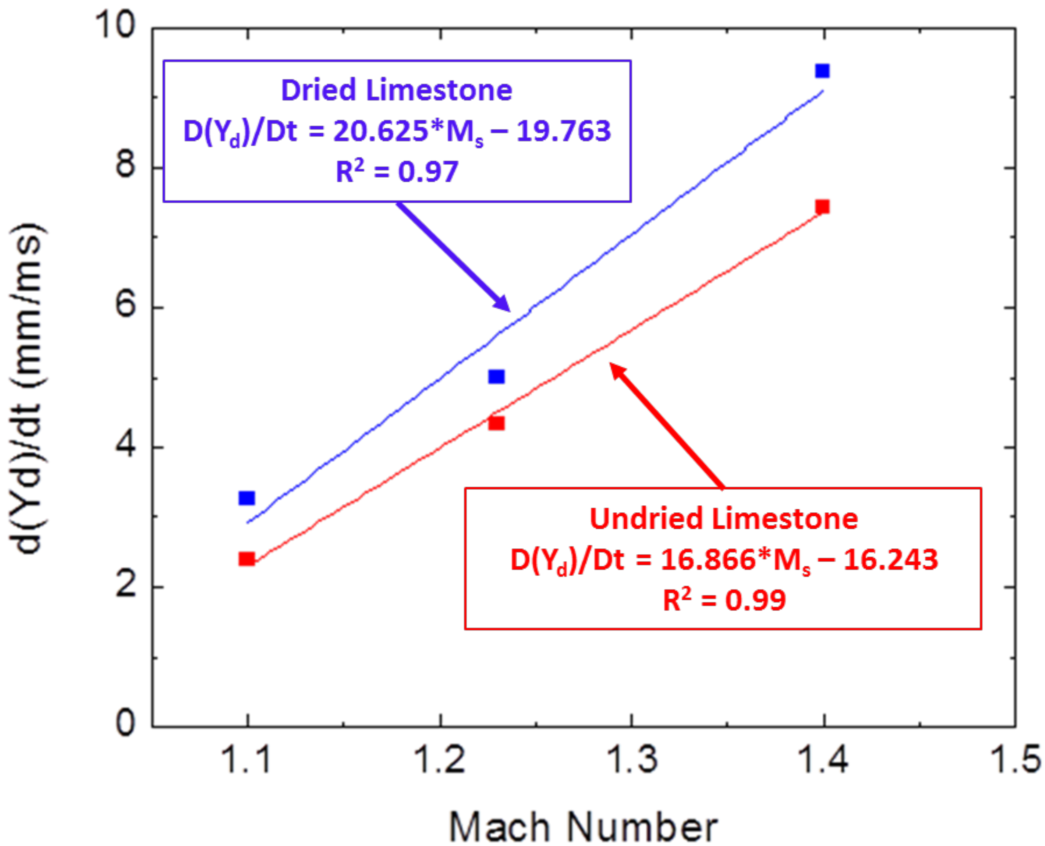

Fig. 6 Dried and undried limestone sample comparison for initial correlated linear growth rates, $\frac{D(Y_d)}{Dt}$, as a function of Mach number, M_s (1.1, 1.23 and 1.4). Dried sample correlations result in larger growth rates, as compared to undried samples at a selected Mach number range from 1.1 to 1.4.

3.2 Conclusion

Limestone samples were represented as both dried and undried samples to discern if differences exist in dust dispersion with varying shock Mach number. The dust-tray volume, which was filled completely with all the limestone sample test cases, remained constant at 60 cm^3. The fixed volume of the dust-tray allowed the mass to vary as the only parameter from sample to sample, which was established by drying the dust and reducing the moisture content.

Overall dust heights were increased from drying the dust, at corresponding Mach numbers. Table 2 summarizes the correlation of dust growth rates with Mach number, delay times for dust to rise after passing normal shock, and transition times from laminar to unstable growth regimes. Note the shock tube dust-tray is recessed 1.45 mm below the camera capture area, and the dust below this level cannot be detected.

Table 2 Correlated values presented in Fig. 6 to predict dust growth rates with known shock Mach numbers ranging from 1.1 to 1.4. Time values indicate dust delay rise times after passing normal shock and transition times from laminar to unstable regimes.

Undried Limestone				Dried Limestone			
Correlation		Critical Times		Correlation		Critical Times	
Mach	$d(Y_d)/dt$ (mm/ms)	Delay Times (ms)	Transition Times (ms)	Mach	$d(Y_d)/dt$ (mm/ms)	Delay Times (ms)	Transition Times (ms)
1.1	2.40	0.27	3.13	1.1	3.27	0.31	3.25
1.23	4.33	0.27	2.01	1.23	5.00	0.16	2.16
1.4	7.44	0.06	1.39	1.4	9.37	0.11	1.31
D(Yd)/Dt	16.866			D(Yd)/Dt	20.625		
Intercept	-16.243			Intercept	-19.763		

Delay times for were greater for dried samples at Mach 1.1 and 1.4, with the opposite trend at Mach 1.23. Transition times were difficult to extract from data, as the exact moment of the laminar transition may vary. Nonetheless, whether the samples are dried or undried, the data shows a decrease in transition times as shock Mach numbers is increased.

Conceivably, the effective moisture reduction in the samples led to fewer agglomerations and/or reduced densities, influencing the ability of lift forces to act on the particles. The moisture-reduced effect increases dust-layer dispersion and growth rates. As the dried limestone clearly increased dust dispersion, this is effectively increasing the likelihood of promoting secondary explosion hazards.

Acknowledgments This work was supported primarily by the Mary Kay O'Connor Process Safety Center at Texas A&M University. Assistance from Dr. Calvin Parnell and his Ph.D. student Balaji Ganesan from the Biological & Agricultural Engineering Department of Texas A&M University for the acquisition of the limestone particle characterization is acknowledged.

References

1. Eckhoff, R. K.: Current Status and Expected Future Trends in Dust Explosion Research, Journal of Loss Prevention in the Process Industries **18**, pp. 225-237 (2005).

2. Houim, R., Oran, E.: Numerical simulation of dilute and dense layered coal-dust explosions, Proceedings of the Combustion Institute **35**, 2083-2090 (2015).

3. Kanno, T., Matsuo, A.: Numerical Investigation of Dust Lifting behind a Shock Wave using LPI Method, Tenth International Symposium on Hazards, Prevention, and Mitigation of Industrial Explosions (X ISHPMIE), Bergen, Norway, 10-14 June (2014).

4. Gerrard, J. H.: An experimental investigation of the initial stages of the dispersion of dust by shock waves, Brit. J. Appl. Phys. **14**, 186-192 (1963).

5. Fletcher, B.: The interaction of a shock with a dust deposit, J. Phys. D: Appl. Phys. **9**, 197-202 (1976).

6. Merzkirch, W., Bracht, K.: The erosion of dust by a shock wave in air: Initial stages with laminar flow, Int. J. Multiphase Flow **4**, 89-95 (1978).

7. Hwang, C. C.: Interaction of a coal dust-bed with shock-induced air stream, W. Merzkirch (ed.), Flow Visualization II, 547-551 (1982).

8. Tateuki, S., Takashi, A.: The effects of particle size on shock wave dust deposit interaction, Proc. of the 14th Intern. Symp. Space Technol. and Sci., 483-490 (1984).

9. Boiko, V. M. and Papyrin, A. N.: Dynamics of the formation of a gas suspension behind a shock wave sliding over the surface of a loose material, Combust. Expl. Shock Waves **23**, 231-235 (1987).

10. Fedorov, A. V.: Mixing in Wave Processes Propagating in Gas Mixtures (Review), Combustion, Explosions and Shock Waves **40**, 17-31 (2004).

11. Klemens, R., Zydak, P., Kaluzny, M., Litwin, D., Wolanski, P.: Dynamics of dust dispersion from the layer behind the propagating shock wave., J. Loss Prev. Process Ind. **19**, 200-209 (2006).

12. Fedorov, A. V., Fedorchenko, I. A.: Computation of Dust Lifting behind a Shock Wave Sliding along the Layer Verification of the Model, Combust., Expl., Shock Waves **41**, 336-345 (2005).

13. Fedorov, A.V., Fedorova, N.N.: Numerical simulations of dust lifting under the action of shock wave propagation along the near-wall layer, J. Phys. IV (France) **12**, Pr. 7-97-Pr. 7-104 (2002).

14. Khmel, T.A., Fedorov, A.V.: Interaction of a shock wave with a cloud of aluminum particles in a channel, Combust. Expl. Shock Waves **38**, 206-214 (2002).

15. Sakakita, H., Hayashi, A. K., Ivandaev A. I.: Numerical simulation of shock wave interaction with powder layers, K. Takayama (ed.), Shock Waves, Springer, Heidelberg (1992).

16. Klemens, R., Wolański, P., Kosiński, P., Korobeinikov, V.P., Semenov, I.V., Markov, V.V., Menshov, I.S.: On combustion and detonation behind a shock wave propagating over dust layer, Khim. Fiz. **20**, 112-118 (2001).

17. Skjold, T., Eckhoff, R.K., Arntzen, B.J., Lebecki, K., Dyduch, Z., Klemens, R., Zydak, P.: Simplified modeling of explosion propagation by dust explosion in coal mines, 5th International Seminar on Fire and Explosion Hazards, Edinburgh, UK, 302-313 (2007).

18. Ilea, C., Kosinski, P., Hoffmann, A.C.: The effect of polydispersity on dust lifting behind shock waves, Powder Technology **196**, 194-201 (2009).

19. Hwang, C.C.: Initial stages of the interaction of a shock wave with a dust deposit, Int. J. Multiphase Flow **12(4)**, 655-666 (1986).

20. Chowdhury, A.Y, Marks, B.D, Johnston, H.G, Mannon, M.S, Petersen, E.L: A New Facility for Studying Shock-Wave Passage over Dust Layers, Shock Waves - An International Journal on Shock Waves, Detonations and Explosions, SHOC-D-14-00095R3 (2015).